HAL open science

Probing PAH Formation from Heptane Pyrolysis in a Single-Pulse Shock Tube

Alaa Hamadi, Leticia Piton Carneiro, Fabian-Esneider Cano Ardila, Said Abid, Nabiha Chaumeix, Andrea Comandini

To cite this version:

Alaa Hamadi, Leticia Piton Carneiro, Fabian-Esneider Cano Ardila, Said Abid, Nabiha Chaumeix, et al.. Probing PAH Formation from Heptane Pyrolysis in a Single-Pulse Shock Tube. Combustion Science and Technology, 2023, 195 (7), pp.1526-1542. 10.1080/00102202.2023.2182199 . hal-04055661

HAL Id: hal-04055661

https://cnrs.hal.science/hal-04055661v1

Submitted on 12 Apr 2023

HAL is a multi-disciplinary open access archive for the deposit and dissemination of scientific research documents, whether they are published or not. The documents may come from teaching and research institutions in France or abroad, or from public or private research centers.

L'archive ouverte pluridisciplinaire **HAL**, est destinée au dépôt et à la diffusion de documents scientifiques de niveau recherche, publiés ou non, émanant des établissements d'enseignement et de recherche français ou étrangers, des laboratoires publics ou privés.

Distributed under a Creative Commons Attribution - NonCommercial 4.0 International License

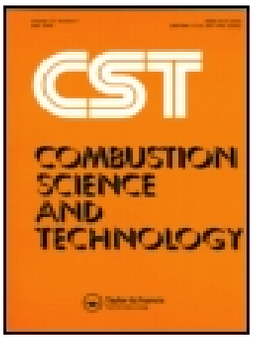

Taylor & Francis
Taylor & Francis Group

Combustion Science and Technology

ISSN: (Print) (Online) Journal homepage: https://www.tandfonline.com/loi/gcst20

Probing PAH Formation from Heptane Pyrolysis in a Single-Pulse Shock Tube

Alaa Hamadi, Leticia Piton Carneiro, Fabian-Esneider Cano Ardila, Said Abid, Nabiha Chaumeix & Andrea Comandini

To cite this article: Alaa Hamadi, Leticia Piton Carneiro, Fabian-Esneider Cano Ardila, Said Abid, Nabiha Chaumeix & Andrea Comandini (2023): Probing PAH Formation from Heptane Pyrolysis in a Single-Pulse Shock Tube, Combustion Science and Technology, DOI: 10.1080/00102202.2023.2182199

To link to this article: https://doi.org/10.1080/00102202.2023.2182199

© 2023 The Author(s). Published with license by Taylor & Francis Group, LLC.

View supplementary material

Published online: 07 Mar 2023.

Submit your article to this journal

Article views: 38

View related articles

View Crossmark data

Full Terms & Conditions of access and use can be found at
https://www.tandfonline.com/action/journalInformation?journalCode=gcst20

COMBUSTION SCIENCE AND TECHNOLOGY
https://doi.org/10.1080/00102202.2023.2182199

Taylor & Francis
Taylor & Francis Group

OPEN ACCESS Check for updates

Probing PAH Formation from Heptane Pyrolysis in a Single-Pulse Shock Tube

Alaa Hamadi[a*], Leticia Piton Carneiro[a*], Fabian-Esneider Cano Ardila[a], Said Abid[a,b], Nabiha Chaumeix[a], and Andrea Comandini[a]

[a]CNRS-INSIS, I.C.A.R.E, Orléans, France; [b]Chemistry Department, Université d'Orléans, Orléans, France

ABSTRACT

To improve our capabilities to model surrogate fuels, particularly in respect to polycyclic aromatic hydrocarbons (PAHs) and soot formation, the pyrolysis of n-heptane is studied in a single-pulse shock across a wide temperature range (900–1700 K) at 20 bar nominal pressure and 4 ms residence time. Three different initial fuel mole fractions are considered, 103, 502, and 2000 ppm of n-heptane in argon. Fuel and intermediate species, including aromatics up to three-ring structures, are measured using gas chromatography and mass spectrometry diagnostics. An ongoing detailed chemical kinetic model for PAH chemistry has been updated to successfully capture the fuel decomposition, the formation of small hydrocarbons, and the concentration of the main PAH products. Major reaction pathways to PAHs are highlighted as well as the role of important intermediate species.

ARTICLE HISTORY
Received 26 July 2022
Revised 12 September 2022
Accepted 16 September 2022

KEYWORDS
Heptane; Pyrolysis; Single-pulse shock tube; Kinetic modeling; Polycyclic aromatic hydrocarbons (PAHs)

Introduction

n-Heptane is widely used as a single-component surrogate for diesel fuel and as a key reference fuel for gasoline (Curran et al. 1998). Thus, its pyrolytic and oxidation chemistry has been studied for decades. At high temperatures, it dissociates into small hydrocarbon products, mainly C_2, C_3, and C_4, which, in absence of oxygen or at fuel-rich conditions, may subsequently react to form larger aromatic species such as the polycyclic aromatic hydrocarbons (PAHs). In general, understanding PAH formation during combustion processes paves the way for the researchers to develop soot formation kinetic models, which can help them improve combustion efficiency and reduce emissions. Hence, a detailed investigation of n-heptane pyrolysis can reveal the fuel breakdown and subsequent molecular weight growth processes.

n-Heptane pyrolysis has long been pursued using numerous experimental configurations and methodologies that cover a wide range of pressure, temperature, and initial fuel concentration conditions. The list of literature investigations concerning n-heptane pyrolysis is reported in Table 1, and it includes only the studies performed in absence of oxygen

CONTACT Alaa Hamadi alaa.hamadi@cnrs-orleans.fr CNRS-INSIS, I.C.A.R.E, 1C, Avenue de la recherche scientifique, Orléans 45071 cedex 2, France; Leticia Piton Carneiro leticia.carneiro-piton@cnrs-orleans.fr CNRS-INSIS, I.C.A.R.E, 1C, Avenue de la recherche scientifique, Orléans 45071 cedex 2, France

*these authors contributed equally

Supplemental data for this article can be accessed online at https://doi.org/10.1080/00102202.2023.2182199

© 2023 The Author(s). Published with license by Taylor & Francis Group, LLC.
This is an Open Access article distributed under the terms of the Creative Commons Attribution-NonCommercial-NoDerivatives License (http://creativecommons.org/licenses/by-nc-nd/4.0/), which permits non-commercial re-use, distribution, and reproduction in any medium, provided the original work is properly cited, and is not altered, transformed, or built upon in any way.

Table 1. Literature review on experimental investigations concerning n-heptane pyrolysis.

Literature	Facility	Conditions	Measured products
(Appleby, Avery, and Meerbott 1947)	flow reactor/multi-isothermal distillation for products determination	NC_7H_{14}, T =823–903 K, p = 1 and 8.7 atm, τ*= not mentioned	C_1-C_4 speciation
(Murata and Saito 1974, 1975)	Flow-tube reactor/gas chromatography	NC_7H_{14} in N_2, T =973 K, p = 1 atm, τ= 0.09 to 46.1 sec.	C_1-C_6 speciation
(Bajus et al. 1979)	Tubular flow reactor/gas chromatography	Steam to n-heptane 3:1, T =953–1033 K, p = 1 atm, τ= 0.14 sec	C_1-C_6 speciation
(Aribike and Susu 1988, 1988)	Annular reactor/gas chromatography	n-heptane in N_2, T =933–1053 K, p = 1 atm, τ= 0.4–1.02 sec	C_1-C_6 speciation
(Pant and Kunzru 1996)	Annular tubular reactor/gas chromatography	n-heptane in N_2, T =953–1023 K, p = 1 atm, τ= 0.08–0.58 sec	C_1-C_6 speciation
(Held, Marchese, and Dryer 1997)	Variable pressure flow reactor/gas chromatography	1430 ppm n-heptane in N_2, T =1085 K, p = 3 atm, τ= 0.6 sec	C_1-C_6 speciation
(Davidson, Oehlschlaeger, and Hanson 2007)	Shock tube/laser absorption	100–500 ppm n-heptane in Ar, T =1100–1560 K, p = 1.6–2 atm	CH_3 concentration time-histories
(Chakraborty and Kunzru 2009)	Tubular reactor/gas chromatography	n-heptane in Ar, T =793–953 K, p = 0.1–2.93 MPa τ= 0.2–14.8 sec	C_1-C_6 speciation
(Garner, Sivaramakrishnan, and Brzezinski 2009)	Shock tube/gas chromatography	100 ppm n-heptane in Ar, T =1000–1350 K, p = 25 and 50 atm, τ= 1–3 ms	C_1-C_5 speciation
(Zamostny et al. 2010)	micro-pyrolysis unit (Shimadzu Pyr-4A)/gas chromatography	2μl n-heptane in N_2, T =1083 K, p = 400 KPa, τ= 0.2–0.4 sec	C_1-C_6 speciation
(Pilla, Davidson, and Hanson 2011)	Shock tube/CO_2 laser for C_2H_4 measurement	300 ppm n-heptane in Ar, T =1350–1950 K, p = 1.3–3.3 atm	C_2H_4 concentration time-histories
(Yuan et al. 2011)	Flow reactor/tunable synchrotron vacuum ultraviolet photoionization mass spectrometry	2% n-heptane in Ar, T =780–1780 K, p = 400 Pa	C_1-C_6 speciation
(Pyun et al. 2013)	Shock tube/DFG laser for CH_4 measurement and CO_2 laser for C_2H_4 measurement	1% n-heptane in Ar, T =1200–1600 K, p = 1.5 atm, τ= 1.5 ms	CH_4 and C_2H_4 concentration time-histories
(Yasunaga et al. 2017, 2018)	Shock tube/gas chromatography	1% n-heptane in Ar, T =1000–1500 K, p = 1–2.5 atm, τ= 1.5–2.2 ms	C_1-C_4 speciation
(Li et al. 2021)	Shock tube/gas chromatography	3% n-heptane in Ar, T =1200–2100 K, p = 2.2–2.8 atm τ= not mentioned	C_1-C_4 speciation

*τ is the reaction time in shock tube experiments and residence time in flow reactor experiments.

as a detailed review on the oxidation chemistry of n-heptane is beyond the scope of the present work.

Among the reported investigations, only few articles provide detailed speciation measurements. The pioneering work by Appleby, Avery, and Meerbott (1947) employed a flow technique to explore the thermal breakdown of n-heptane between 823 and 903 K at pressures of 1 and 8.7 atm. Murata and Saito (1974, 1975) studied the decomposition of paraffins and 1-olefins, including n-heptane, at 973 K and 1 atm, and developed a molecular model to explain the product distribution. Both Bajus et al. (1979), Pant and Kunzru (1996), and Chakraborty and Kunzru (2009) examined the steam cracking of n-heptane and determined the overall breakdown rate, by monitoring the formation of stable small hydrocarbon products using gas chromatography. Aribike and Susu (1988, 1988) proposed a mechanistic model for n-heptane pyrolysis based on product distribution data acquired in a pulse reactor at atmospheric pressure and reaction durations of 0.40–1.02 s at 933–1053 K. Held and his coworkers (1997) developed a simplified high-temperature pyrolysis and oxidation model for n-heptane that is validated against a variety of datasets, including their flow reactor experiments. More recent investigations have employed shock tube techniques for kinetic studies. Various time-history measurements were performed at Stanford University focusing on CH_3 (Davidson, Oehlschlaeger, and Hanson 2007), C_2H_4 (Pilla, Davidson, and Hanson (2011) and Pyun et al. (2013)), and CH_4 (Pyun et al. 2013) products. The single-pulse technique coupled to gas chromatography was also employed by Garner, Sivaramakrishnan, and Brzezinski (2009) to investigate the pyrolysis of saturated and unsaturated C_7 hydrocarbons, including n-heptane, in the temperature range 1000–1350 K at pressures of 25 to 50 atm with reaction times of 1–3 ms using a high-pressure shock tube. Yasunaga et al. (2017, 2018) carried out a series of works to address the decomposition of 1% n-heptane in argon using a single-pulse shock tube at pressures of 1.0–2.5 atm and temperatures of 1000–1500 K for reaction durations ranging from 1.5 to 2.2 ms. Li et al. (2021) conducted n-heptane and iso-octane pyrolysis experiments in a shock tube across a temperature range of 1200–2100 K and pressure range of 2.2–2.8 atm. Finally, among other techniques, Yuan et al. (2011) reported speciation measurements in n-heptane pyrolysis at low pressure (400 Pa) and temperatures ranging from 780 to 1780 K using a flow reactor and synchrotron vacuum ultraviolet photoionization mass spectrometry.

According to the above review, past research has focused on the fuel decomposition reactivity and the formation of small hydrocarbons up to C_6 intermediates. No studies have been conducted to investigate the formation of PAHs from n-heptane pyrolysis, though this latter focus is highly required for the development of clean combustion technologies. For this reason, the present work aims to provide shock tube speciation datasets spanning from small hydrocarbons to three-ring aromatics from n-heptane pyrolysis experiments at conditions relevant to modern combustion devices (20 bar, 900–1770 K). Our most recent kinetic model (Hamadi et al. 2022) has been updated to simulate and interpret the newly obtained experimental data. Kinetic insights into the formation of aromatic molecules from n-heptane pyrolysis will be addressed based on the experimental findings and kinetic modeling analyses.

Shock tube pyrolysis experiments

Pyrolysis experiments with three different n-heptane concentrations are performed using the high-purity single-pulse shock tube facility with dilute mole fractions of 103 ppm, 502 ppm, and 2000 ppm in bulk argon. A detailed description of the shock tube apparatus is well documented in our previous publications (Sun et al. 2022), so only a brief description is given here. The single-pulse shock tube apparatus consists of the driven (length: 6 m; inner diameter: 78 mm) and the driver (length: 3.7 m; inner diameter: 120 mm) sections, separated by a double diaphragm. The shock tube is equipped with a dump tank (volume 150 L) located near the diaphragm section, making it operate in a single pulse fashion. The low-pressure section is heated to 90°C to avoid condensation (or absorption) of fuel and reaction products. It is also pumped down to below 10^{-5} mbar with a turbo-molecular pump before each experiment. To avoid carbon deposits, the inner surface of the shock tube is cleaned regularly.

Four pressure sensors (CHIMIE METAL A25L05B) are mounted on the side wall of the driven section. The adjacent sensors are 150 mm apart, and the last sensor is 82 mm from the end wall. The distance and time difference between two successive pressure sensors are used to calculate the average incident shock velocity, which is then used to determine T_5 and p_5 behind the reflected shock wave by solving the conservation equations (Hugoniot 1887, 1889; Rankine 1870). The calculated T_5 is subject to an uncertainty of ± 30 K due to the attenuation of the shockwave and the physical dimension of the pressure sensors (Hamadi et al. 2022). A PCB Piezotronics pressure sensor, shielded by a layer of room-temperature vulcanizing (RTV) silicone, is located on the end wall of the driven section to record the pressure history of each shock, from which the corresponding reaction time is determined (Tang and Brezinsky 2006). The reaction time for each experiment is defined as the time interval between the arrival of the incident shock wave and the time point at which the pressure drops to 80% p_5 as a result of the quenching rarefaction waves. For the current experimental configuration, the nominal reaction time is 4 ms.

Stable species are withdrawn from the shock tube via an air-actuated valve and analyzed by the analytical system, which consists of three parts: an Agilent GC series 7890B, a Thermo Trace GC Ultra, and a Thermo DSQ mass spectrometer. The Agilent GC, designed to measure PAHs up to four rings, is equipped with a flame ionization detector (FID) coupled to a DB-17 ms column for heavy species separation, and a thermal conductivity detector coupled to a Molsieve 5A column for monitoring the absence of air and the dilution level by helium. An external valve box, coupled to the Agilent GC, diminishes the heavy compounds loss during sample storage and injection by maintaining the temperature at 320°C. The Thermo Trace GC is also equipped with an FID detector, connected to a HP Plot Q column for measuring light species up to mono-aromatics. The gas samples were also injected into the DSQ mass spectrometer, but in this case the MS analyses did not provide any additional information as all the heavy PAH compounds detected had been previously identified in our sequential studies on aromatic fuels.

The quantification of the measured species is based on the calibrations of the FID responses performed before the experiments. Standard gas mixtures are used for the calibration of the light species representing the C_1-C_5 hydrocarbons except for diacetylene (C_4H_2) and triacetylene (C_6H_2), whose calibration factors are obtained from high-temperature acetylene (C_2H_2) pyrolysis experiments through carbon atom conservation. Similarly,

liquid fuels are used to calibrate benzene, heptane, toluene, styrene, and phenylacetylene. For all of the above calibrations, mixtures are prepared in stainless steel vessel using the partial pressure method. For small PAHs up to three rings, the calibration procedure differs. Here, the calibrations use gas-phase mixtures prepared in a heated glass vessel (200°C) (Sun et al. 2021b) to minimize surface adsorption (Comandini, Malewicki, and Brezinsky 2012). Uncertainties in species mole fractions are 5% for directly calibrated small species and 10% to 15% for PAH species calibrated in the gas phase. These uncertainties derive from the reproducibility of the single measure when repeated several times and the uncertainties in the composition of the initial reference calibration mixtures which reflect in the accuracy of the calibration curves.

The experiments are conducted with helium (Air Liquide, purity>99.995%) as the driver gas and dilute mixtures of n-heptane (Sigma – Aldrich, purity≥99.5%) in argon bath gas (Air Liquide, purity>99.9999%). The experimental gas mixtures are prepared in a 136 L electropolished stainless-steel cylinder that is evacuated in advance below 10^{-5} mbar with a turbomolecular pump. Before performing the experiments, the prepared gas mixtures are left overnight to homogenize, and the actual pre-shock compositions are analyzed by GC. The ***Supplementary Material*** provides all experimental results, consisting of the post-shock conditions (T_5, p_5), the measured pressure profiles, the defined reaction time, and the mole fraction measurements for individual species.

Kinetic modeling

The current work is a continuation of our previous serial work to build a kinetic model that can accurately predict the pyrolytic PAH formation under high-pressure and temperature conditions (the last version being published in (Hamadi et al. 2022)). The n-heptane sub-mechanism of Zhang et al. (2016) is chosen as a substitute for the lumped heptane chemical mechanism. The n-heptane sub-mechanism involves unimolecular decomposition and H-abstraction reactions from the fuel and the corresponding fuel radicals. The reactions of cyclohexadiene with molecular hydrogen (CYC_6H_8+H) and subsequent fragmentation and the corresponding rate coefficients reported in (Wang, Villano, and Dean 2015) are incorporated into the current kinetic model. The rate coefficients of the unimolecular decomposition reaction of 1-pentene (C_5H_{10}-1) and 1-hexene (C_6H_{12}-1) are an update from the work of (Shao et al. 2020). Additionally, the rate coefficients of the H-abstraction reaction of ethylene (C_2H_4) are taken from the same LLNL PAH model (Shao et al. 2020).

Thermochemical data for most species are from the CRECK model (Pejpichestakul et al. 2019), as it is the basis of the current model (Sun et al. 2021c). For species introduced by reactions added or updated in this work, the thermochemical data are from the same publications. The mechanism file and thermochemical data for the current kinetic model are provided in the Supplementary Material.

All simulations in the present work are performed using the homogeneous reactor model of the COSILAB software. The nominal reaction time of 4.0 ms and constant pressure of 20 bar are used for the simulations. The assumption of constant pressure, typically used in simulations of speciation results from single-pulse shock tube experiments, has been well justified in previous publications (Han, Mehta, and Brezinsky 2019; Tang and Brezinsky 2006). However, it is suggested that certain reactions involving resonantly stabilized radicals may occur during the post-shock quenching period, resulting in an increase in the mole

fractions of some products (Manion, Sheen, and Awan 2015; Mertens et al. 2018). In addition, depending on the characteristics of the experimental facility (small-bore shock tubes) or conditions (higher fuel concentrations) (Ferris, Davidson, and Hanson 2018; Mehta, Wang, and Brezinsky 2022), the constant-pressure assumption may be erroneous. Simulations with measured pressure profiles are performed over a longer time period (10.0 ms) for all n-heptane sets. The time-dependent concentrations of the major products and important radicals are shown in Figure S1 in the Supplementary Material. The plateaus in the concentration profiles of the main products are reached before the quenching process which indicates that their formation is already completed at the specified reaction time. The reaction systems currently studied do not produce large amounts of highly stabilized radicals such as propargyl and benzyl, so their concentrations are too low to significantly affect the amount of final products as shown in Figures S2-S4.

Similar to the vast literature on n-heptane experimental chemistry, several detailed kinetic models have been developed and optimized in the past decades based on the available data. Some of the most recent models, such as NUIG (Zhang et al. 2016), JetsurFv2 (Wang et al. 2010), CRECK (Pejpichestakul et al. 2019), and LLNL PAH (Shao et al. 2020), were also used to simulate the current experiments for comparison purpose (Figures S5–S7). The current model is compared to NUIG and JetsurFv2 for small hydrocarbon predictions, as well as the CRECK and LLNL PAH models for both small hydrocarbon and aromatic species predictions. In comparison to the other tested models, the LLNL PAH model is in good agreement with our experiments except for over-predictions for benzene, phenylacetylene, and naphthalene.

The current kinetic model for heptane pyrolysis is tested against pertinent speciation data reported in literature to assess its capability to predict results under different conditions (Garner, Sivaramakrishnan, and Brzezinski 2009; Held, Marchese, and Dryer 1997; Yasunaga et al. 2017, 2018; Yuan et al. 2011). There are a variety of experimental setups and, as a result, simulation methodologies involved. For the shock tube experiments (Garner, Sivaramakrishnan, and Brzezinski 2009; Yasunaga et al. 2017, 2018), each data point is simulated with the "homogeneous reactor" by entering the measured T_5, p_5 and reaction time. The "plug-flow" model is employed to simulate heptane pyrolysis speciation in a flow tube (Yuan et al. 2011). As for the experiments performed with the variable-pressure flow reactor (Held, Marchese, and Dryer 1997), an isobaric and adiabatic zero-dimensional reactor is used to simulate the species mole fraction time histories by providing the initial temperature, pressure, and chemical compositions. Figures S8–S12 in the Supplementary Material show the comparisons between the literature data and the simulations with the current model.

Results and discussions

In this section, experimental and simulated species concentrations as a function of post-shock temperature T_5 will be compared to validate the prediction capabilities of the present kinetic model. Only the data from 502 and 2000 ppm of n-heptane are presented in the discussion, while the ones for 103 ppm are given in Figure S2 in the Supplementary Material. In general, the model can mimic the mole fraction profiles of observed pyrolysis species and capture their decomposition and formation temperature windows within the experimental errors. To gain insight into the chemistry of heptane degradation and

aromatics growth, modeling analytical approaches such as rate of production (ROP) analyses and sensitivity analyses are applied.

Fuel decomposition and the formation of small hydrocarbons

Figure 1 presents the experimental and simulated mole fraction profiles of n-heptane and C_1–C_6 acyclic species in the three separate sets. The kinetic model satisfactorily predicts the measured fuel conversion profiles as well as the formation of small intermediates in the individual studied cases. Olefins begin to form during the early stage of the fuel consumption. To determine the relationship between various alkene production and fuel consumption, Figure 2 displays initial fuel consumption pathways based on integrated rate-of-production (ROP) analyses over 4 ms in the three reaction systems. The temperatures chosen to perform these ROP calculations are 1160 K for 103 and 502 ppm heptane pyrolysis, and 1130 K for 2000 ppm heptane pyrolysis, where roughly half of the fuel is consumed in each case. The reaction scheme shows that n-heptane is largely consumed via the H-abstraction reactions, which produce 1-, 2-, 3-, and 4-heptyl radicals, and via the C-C bond scission reaction, which produces n-propyl (NC_3H_7) and 1-butyl (PC_4H_9) radicals. Other C-C bond fission reactions that produce methyl and 1-hexyl radicals, as well as ethyl and 1-pentyl radicals, contribute only slightly to the thermal decomposition of n-heptane. Following the decomposition of the major heptane radicals, the various alkene

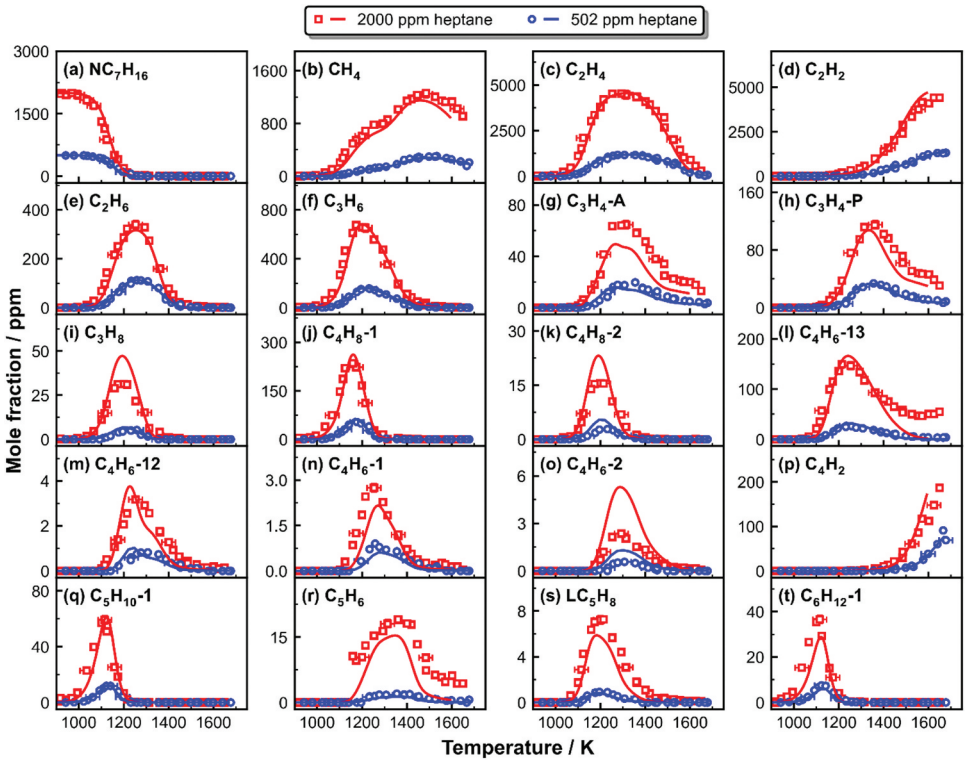

Figure 1. Measured (symbols) and simulated (lines) mole fraction profiles of fuel and small intermediates as a function of post-shock temperature T_5 in heptane pyrolysis.

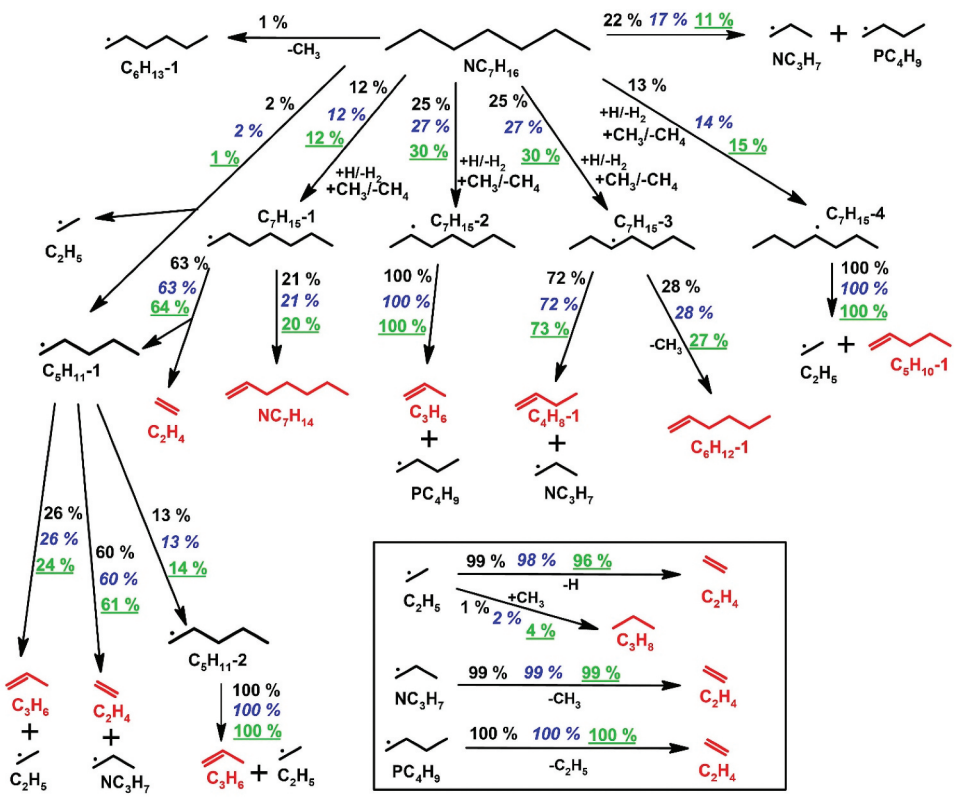

Figure 2. Fuel consumption pathways at 1160 K in 103 and 502 ppm n-heptane pyrolysis and at 1130 K in 2000 ppm n-heptane pyrolysis, 20 bar. The percentage numbers (103 ppm heptane: black normal; 502 ppm heptane: blue italic; 2000 ppm heptane: green underlined) are the contributions by the corresponding reactions to the consumption of the species on the source side. The reaction path analyses are based on the integrated ROP analyses over 4 ms.

products are produced. Propylene (C_3H_6, Figure 1f) and 1-pentene (C_5H_{10}-1, Figure 1q) are directly formed through the unimolecular decomposition of 2- and 4-heptyl radicals, respectively (see Figure 2). The 3-heptyl radical allows a modest but significant fraction of methyl radical (CH_3) and l-hexene (C_6H_{12}-1, Figure 1t) to be formed in favor of NC_3H_7 and l-butene (C_4H_8-1, Figure 1j). The allyl (C_3H_5-A)+CH_3 recombination reaction is the second important C_4H_8-1 formation channel at 1160 K (around 30% according to the ROP analyses). C_3H_5-A is produced mostly from the unimolecular decomposition of C_5H_{10}-1 (C_5H_{10}-1= ethyl (C_2H_5) + C_3H_5-A) and C_6H_{12}-1 (C_6H_{12}-1= NC_3H_7+ C_3H_5-A), and partly from the C_3H_6 through H-abstraction reactions with methyl radical and hydrogen atom. The other butene isomer, 2-butene (C_4H_8-2, Figure 1k), is produced mainly through isomerization and H-assisted isomerization of C_4H_8-1, with increasing contribution from C_5H_{10}-1 + CH_3 reaction along with the initial fuel concentration (from 10% with 103 ppm to 30% with 2000 ppm initial n-heptane mole fraction at 1170 K). Ethylene (C_2H_4, Figure 1c) is formed via numerous reaction pathways as shown in Figure 2, including 1-heptyl decomposition, thermal decomposition of the 1-pentyl (C_5H_{11}-1), 1-butyl, l-propyl and ethyl radicals formed in 1-,2-,3-and 4-heptyl decomposition, respectively, and further H-abstraction reactions of the other olefinic

intermediates, namely C_3H_6 and C_4H_8-1. The dominant C_2H_4 consumption route is the unimolecular fragmentation into vinyl radicals (C_2H_3) and H-atoms. Aside from alkenes, the recombination of methyl and ethyl drives propane formation (C_3H_8, Figure 1i), which starts at the early phases of heptane decay. Pentadiene (LC_5H_8, Figure 1s) is the result of the unimolecular decomposition of pentenyl (NC_5H_9-3) and heptenyl radicals (NC_7H_{13}), which are formed through dehydrogenation of C_5H_{10}-1 (Figure 1q) and 1-heptene (NC_7H_{14}), respectively. NC_7H_{14} (not measured in the current study) is produced entirely by the unimolecular breakdown of C_7H_{15}-1 (Figure 2).

The remaining small hydrocarbons are formed through subsequent reactions. The remarkable mole fractions of methane (CH_4) and ethane (C_2H_6) in n-heptane pyrolysis (Figure 1 b, e, respectively) arise from the abundant CH_3 production via $NC_3H_7 = CH_3 + C_2H_4$ reaction at low temperatures (>1200 K), $H + C_3H_6 = CH_3 + C_2H_4$ reaction at moderate temperatures (1200–1350 K), and unimolecular decomposition of C_2H_6 at high temperatures (>1400 K). Acetylene (C_2H_2, Figure 1d) is predominantly formed by the decomposition of C_2H_3 and marginally by the reaction of H atoms with allene (C_3H_4-A, Figure 1g) and propyne (C_3H_4-P, Figure 1h). The C_3H_4 isomers, C_3H_4-P and C_3H_4-A, are formed at temperatures where the fuel is nearly depleted. C_3H_6 consumption leads to C_3H_4-A, which isomerizes to C_3H_4-P. Four C_4H_6 isomers are observed: 1-butyne (1-C_4H_6, Figure 1n), 2-butyne (2-C_4H_6, Figure 1o), 1,2-butadiene (1,2-C_4H_6, Figure 1m) and 1,3-butadiene (1,3-C_4H_6, Figure 1l). Quantitative mole fraction profiles for C_4H_6 isomers are rarely reported in previous investigations on n-heptane pyrolysis. The current model captures 1,3-C_4H_6, 1,2-C_4H_6, and 1-C_4H_6 profiles well; nevertheless, discrepancies exist between the experimental and simulated 2-C_4H_6 speciation profiles with an overprediction of the experimental profiles. The peak mole fraction of 1,3-C_4H_6 is fifty times greater than that of the other three isomers. ROP analyses are done across the temperature formation windows to better explain the higher peak mole fractions of 1,3-butadiene. The formation of the dominant isomer 1,3-C_4H_6 largely relies on the 1-C_4H_8 consumption through the stepwise dehydrogenation via 1-buten-3-yl (C_4H_71–3) radical as an intermediate. As we observed above, 1-butene is one of the main alkenes from the direct decomposition of the heptyl radicals, thus its large concentrations (Figure 1j) drive the formation of 1,3-C_4H_6. The other C_4H_6 isomers are mainly produced by bimolecular recombination reactions. 1,2-C_4H_6 is mainly formed through CH_3 + propargyl (C_3H_3) reaction, where C_3H_3 is produced from the decomposition of C_3H_4-P and C_3H_4-A. Reactions between CH_3 and C_3 molecules/radicals (C_3H_4-A and C_3H_3) govern the formation of 1-C_4H_6. The production of 2-C_4H_6 mostly depends on the isomerization reactions of 1,2-C_4H_6 and just moderately by 1,3-C_4H_6 isomerization reactions. Regarding C_5 species, cyclopentadiene (C_5H_6, Figure 1r) is mainly produced through the dehydrogenation of cyclopentene (CYC_5H_8) and slightly through the reaction C_3H_5-A+C_4H_6=C_2H_5+C_5H_6. The 1-penten-4-yl radical ($C_5H_9$14) formed by the C_3H_5-A+C_2H_4 recombination reaction can undergo cyclization reaction to produce cyclopentenyl radical (cyC_5H_9), which is the main source of CYC_5H_8 through its β-C – H scission. Though not shown in Figure 1, CYC_5H_8 mole fractions are measured in our investigation and are available in the Supplementary Material.

Aromatic growth

Figure 3 depicts the experimental and simulated mole fraction profiles of several common mono-aromatic hydrocarbons (MAHs) and bicyclic and tricyclic PAHs. For all the aromatics, the current model accurately captures the experimental trends regarding the shapes and the peak concentrations. The major aromatic formation pathways are identified through ROP analyses and will be addressed in this section. The reactions that account for the formation of these aromatics are similar in all the reaction systems; however, the product concentrations increase with the fuel mole fraction due to the increased amount of carbon in the reaction system.

One of the key subjects covered in kinetic studies of acyclic fuel consumption under fuel-rich or pyrolytic conditions is the production of the first aromatic ring. The MAH species detected in n-heptane pyrolysis include benzene (C_6H_6), toluene (C_7H_8), phenylacetylene ($C_6H_5C_2H$), styrene ($C_6H_5C_2H_3$), and ethylbenzene ($C_6H_5C_2H_5$). C_6H_6 (Figure 3a) is the most abundant MAH species formed during n-heptane pyrolysis. Integrated ROP analyses at 1250 K and 1450 K are used to identify the reaction pathways leading to C_6H_6 production as shown in Figure 4. Three sources are responsible for C_6H_6 production in heptane pyrolysis: the dehydrogenation of 1,4-cyclohexadiene (CYC_6H_8) that is mainly produced from C_2H_3+C_4H_6 recombination followed by cyclization, H-abstraction and β-scission (Wang, Villano, and Dean 2015), the reaction sequence $2C_3H_3 \rightarrow$ fulvene$\rightarrow C_5H_5CH_2$-1/ $C_5H_5CH_2$-2 $\rightarrow C_6H_6$ (Miller and Klippenstein 2003), and the C_3H_3 self-recombination. The relative importance of the above-mentioned channels varies with temperature. The first two pathways control C_6H_6 formation in the low-temperature range of our study, whereas the latter two at higher temperatures. It is worth mentioning how the pathway through

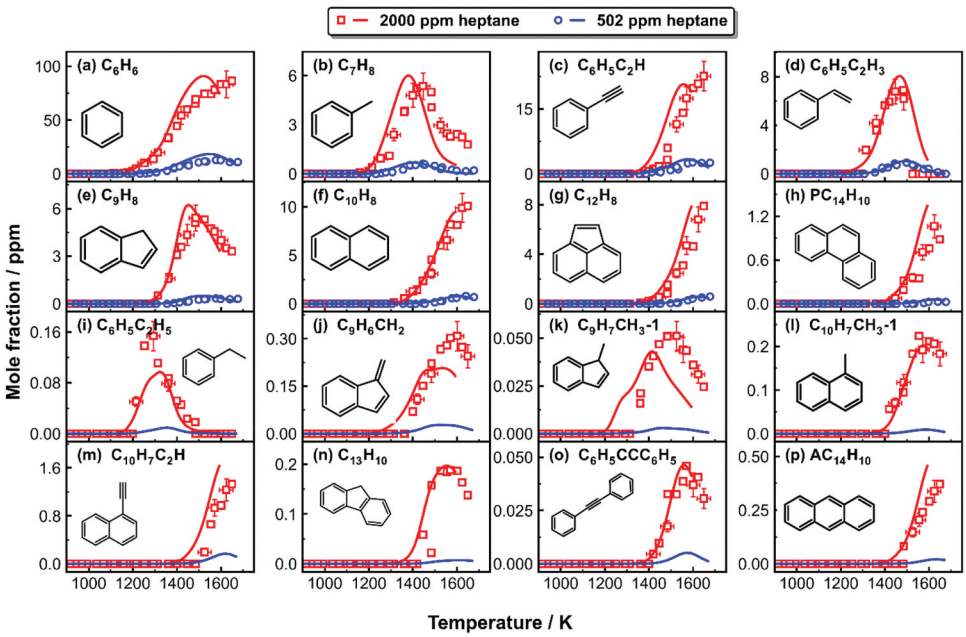

Figure 3. Measured (symbols) and simulated (lines) mole fraction profiles of MAHs and PAHs as a function of post-shock temperature T_5 in n-heptane pyrolysis.

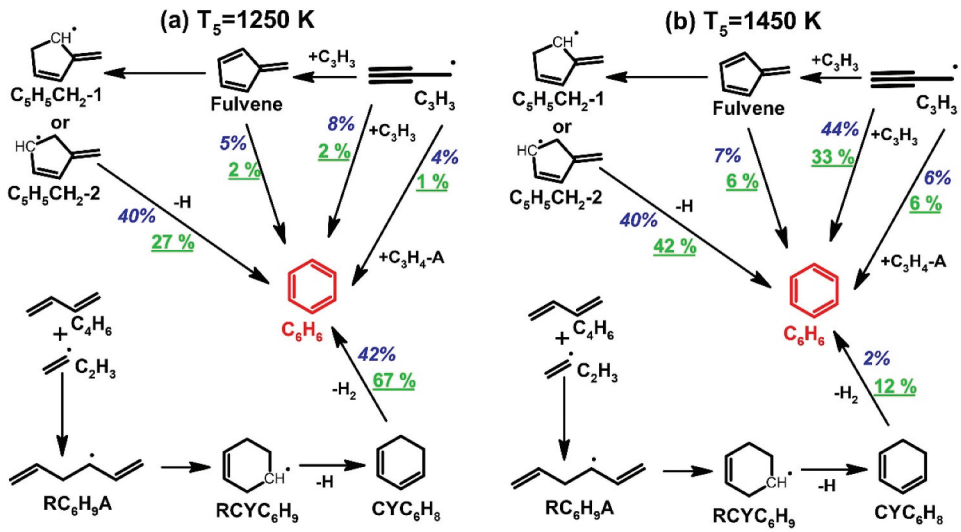

Figure 4. The reaction pathways leading to benzene formation at (a) T_5 = 1250 K, (b) T_5 = 1450 K in the pyrolysis of n-heptane. The percentage numbers (502 ppm heptane: blueitalic; 2000 ppm heptane: green underlined) represent the contributions to benzene formation by the corresponding reactions.

1,4-cyclohexadiene is also strongly dependent on the initial fuel concentration. Besides, the C_3H_5-A+C_3H_3 recombination and the fulvene isomerization have minor contributions to C_6H_6 throughout the temperature range (see Figure 4).

The formation of C_7H_8 (Figure 3b) largely depends on the reactions of C_3H_3 with C_4H_6 and but-2-yn-1-yl radical (C_4H_5-2), respectively. The formation of $C_6H_5C_2H$ (Figure 3c) and $C_6H_5C_2H_3$ (Figure 3d) mostly relies on the reactions of phenyl with C_2H_2/C_2H and C_2H_4, respectively. C_5H_5+C_3H_3 reaction and C_4H_6 self-recombination also slightly contribute to $C_6H_5C_2H_3$ at low temperatures. $C_6H_5C_2H_5$ is mainly formed through benzyl (C_7H_7)+CH_3. C_4H_6 self-recombination also has a non-negligible contribution to $C_6H_5C_2H_5$.

The major goal of this work is to unravel the mechanisms responsible for PAH formation during n-heptane pyrolysis. The smallest PAH detected in this study is indene (C_9H_8, Figure 3e). C_9H_8 mainly originates from the bimolecular reaction C_9H_7+H=C_9H_8 at low temperatures (T_5<1400 K), where C_9H_7 is exclusively formed from C_4H_2+C_5H_5 reaction. As the temperature increases, the isomerization of 1-phenyl-propyne ($C_6H_5C_3H_3$P_1) and phenyl-allene ($C_6H_5C_3H_3$A) and C_7H_7+C_2H_2 reaction become the dominant C_9H_8 formation channels. The corresponding rate parameters have been validated in our previous investigations on the pyrolysis of propylene and propyne (Sun et al. 2021a), and C_2 and C_3 addition to toluene and benzene (Hamadi et al. 2022; Sun et al. 2021a, 2022). $C_6H_5C_3H_3$P_1 is largely formed through the molecule+radical reaction $C_6H_5C_2H$+CH_3, whereas the radical+radical reaction C_6H_5+C_3H_3 is the major source of $C_6H_5C_3H_3$A.

C_9H_8 consumption mostly yields indenyl radical (C_9H_7) through H-abstraction and unimolecular decomposition. C_9H_7 participates in the formation of the other PAHs, including naphthalene ($C_{10}H_8$) and acenaphthylene ($C_{12}H_8$), which were found to be the most prevalent in the current study (Figure 3f,g). The formation mechanism of $C_{10}H_8$

includes several possible reaction pathways that are displayed in Figure 5 based on ROP analysis done at 1525 K. As can be seen in Figure 5, benzofulvene ($C_9H_6CH_2$) is a vital precursor of naphthalene. According to the ROP-analyzed results, the formation of $C_9H_6CH_2$ relies on three major channels: i) the unimolecular decomposition of methyl-indene radical ($C_9H_6CH_3$-1) following the production of 1-methyl-indene ($C_9H_7CH_3$-1) through C_9H_7+CH_3 recombination; ii) the recombination between fulvenallyl (C_7H_5) and C_3H_3. (C_7H_5 mainly comes from C_7H_7 decomposition and the C_3H_3+C_4H_2 recombination); iii) the bimolecular reaction between o-benzyne (o-C_6H_4) and vinylacetylene (C_4H_4). (o-C_6H_4 is mostly derived from C_7H_7 breakdown). Besides the isomerization of benzofulvene, other potential sources of naphthalene include the consumption of methyl-indene radicals ($C_9H_7CH_2$ and $C_9H_6CH_3$-1), C_7H_5+C_3H_3 reaction, and the hydrogen abstraction acetylene addition (HACA) route through phenylacetylene radical ($C_6H_4C_2H$) leading to naphthyl ($C_{10}H_7$) radicals which will recombine with H atom (not shown in Figure 5).

1-methyl-indene ($C_9H_7CH_3$-1), 1-methyl naphthalene ($C_{10}H_7CH_3$-1), acenaphthylene ($C_{12}H_8$), 1-ethynyl-naphthalene ($C_{10}H_7C_2H$_1) and fluorene ($C_{13}H_{10}$) are among the major C_{10}–C_{13} PAHs identified in this study. As previously stated, $C_9H_7CH_3$-1 (Figure 3k) is a key precursor for the naphthalene-benzofulvene isomer pair. The C_9H_7+CH_3 recombination produces the majority of $C_9H_7CH_3$-1. $C_{12}H_8$ (Figure 3g) is one of the most abundant PAHs in n-heptane pyrolysis. The C_9H_7+C_3H_3 recombination and the subsequent dehydrogenation and ring-rearrangement processes (Jin et al. 2019) prevails $C_{12}H_8$ formation throughout the temperature range. The formation of the remaining PAHs involves the participation of naphthyl radical ($C_{10}H_7$-1): $C_{10}H_7$-1+CH_3 recombination is the primary source of $C_{10}H_7CH_3$-1 (Figure 3l); the HACA route $C_{10}H_7$-1+C_2H_2 = $C_{10}H_7C_2H$_1+H controls the

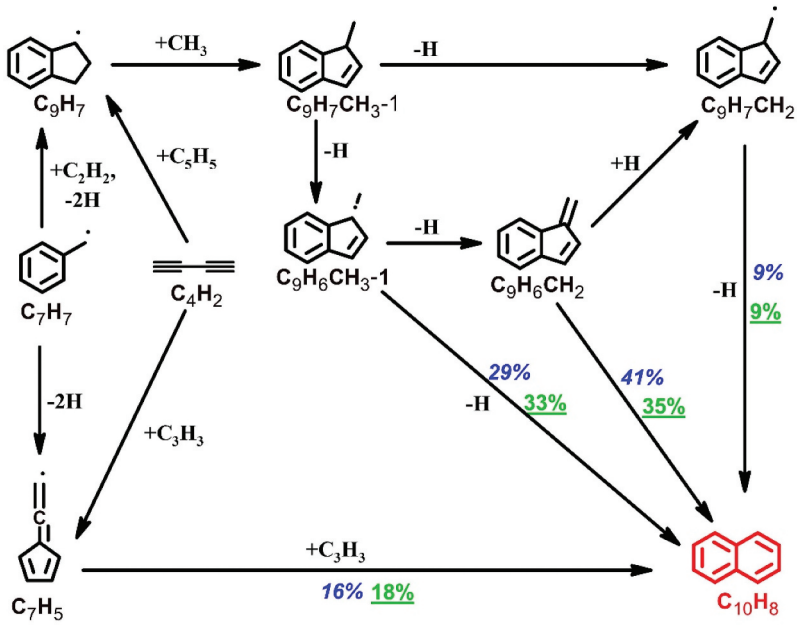

Figure 5. The reaction pathways leading to naphthalene formation at T_5 = 1525 K in the pyrolysis of heptane. The percentage numbers (502 ppm heptane: blue italic; 2000 ppm heptane: green underlined) represent the contributions to naphthalene formation by the corresponding reactions.

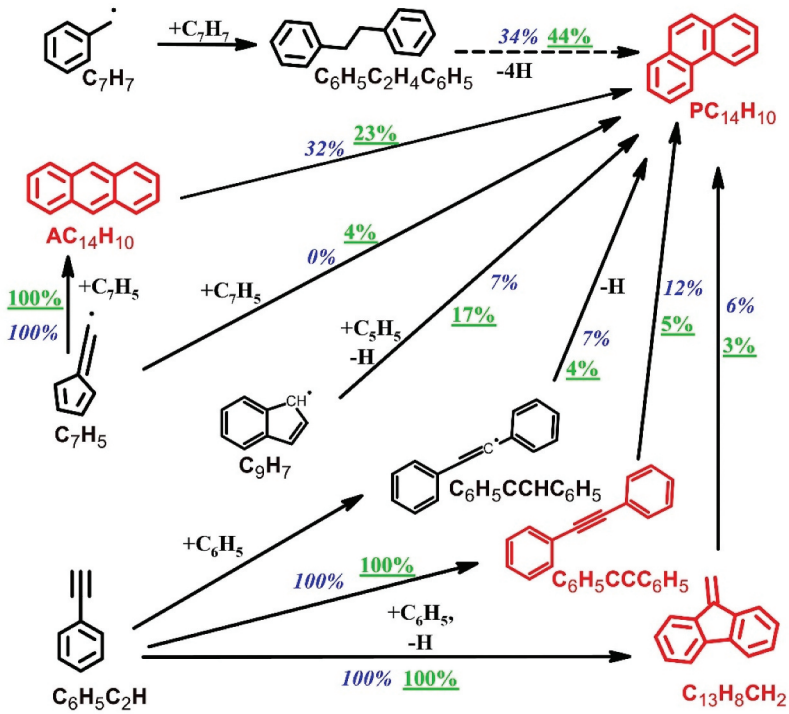

Figure 6. The reaction pathways leading to the formation of $C_{14}H_{10}$ isomers at T_5 = 1500 K in the pyrolysis of n-heptane. The percentage numbers (502 ppm n-heptane: blue italic; 2000 ppm n-heptane: green underlined) represent the contributions to $C_{14}H_{10}$ isomers formation by the corresponding reactions. The dashed arrows represent multi-step reaction.

formation of $C_{10}H_7C_2H$_1 (Figure 3m) and it also partly accounts for $C_{12}H_8$ formation (27% at 1525 K); $C_{10}H_7$-1+C_3H_4-P is a minor route leading to $C_{13}H_{10}$ (Figure 3n). In this case, the C_9H_7+vinylacetylene (C_4H_4) reaction governs the $C_{13}H_{10}$ formation throughout the temperature range.

Four different $C_{14}H_{10}$ species are identified and quantified in 2000 ppm heptane pyrolysis, including the dominant phenanthrene ($PC_{14}H_{10}$), and its isomers, diphenylacetylene ($C_6H_5CCC_6H_5$), 9-methylene-fluorene ($C_{13}H_8CH_2$), and anthracene ($AC_{14}H_{10}$). Reaction pathways leading to $C_{14}H_{10}$ isomers formation at 1500 K are presented in Figure 6. $C_6H_5CCC_6H_5$ (Figure 3o) and $C_{13}H_8CH_2$ (not shown in Figure 3) are the products of the $C_6H_5C_2H$+C_6H_5 addition-elimination reaction (Sun et al. 2020). $AC_{14}H_{10}$ (Figure 3p) is totally formed from C_7H_5 self-recombination. $PC_{14}H_{10}$ (Figure 3h) mainly comes from the C_7H_7 self-recombination and $AC_{14}H_{10}$ isomerization. Other reaction channels which contribute to $PC_{14}H_{10}$ formation include: the C_7H_5 self-recombination, H-assisted isomerization of $C_6H_5CCC_6H_5$ and $C_{13}H_8CH_2$, and the reaction of C_9H_7 with cyclopentadienyl radical (C_5H_5), which results from the consumption of C_5H_6 and the addition of C_3H_3 to C_2H_2.

Conclusion

This research highlights PAH products from n-heptane pyrolysis as a significant new contribution to the literature on the chemistry of this important surrogate component. The experiments were carried out in a single-pulse shock tube coupled to gas chromatographic techniques at a nominal pressure of 20 bar throughout a temperature range of 900–1700 K. Updates to our ongoing PAH kinetic model demonstrate satisfactory predictive performances for the speciation measurements obtained in this work as well as those reported in literature studies on n-heptane pyrolysis. Heptane mainly decomposes through C-C fission and H-abstraction reactions leading to the formation of heptyl, n-butyl and n-propyl radicals. These Alkyl radicals further undergo beta-fission reactions leading to the formation of alkenes, namely, ethylene, propylene, 1-butene, 1-pentene and 1-hexene. The consumption of alkenes results in key intermediates such as methyl, acetylene, ethyl, propargyl, and 1,3-butadiene, which play a significant role in the formation and growth of aromatics. In particular, the formation of benzene relies on C_2H_3+C_4H_6 reaction through the intermediate cyclohexene, the H-addition and isomerization of fulvene, and C_3+C_3 reactions, more specifically, propargyl self-recombination and propargyl+allene reaction. Toluene is the product of the addition reaction of C_3H_3 to 1,3-butadiene. Indene formation mainly depends on C_4H_2+C_5H_5 reaction at low temperatures and on the consumption of $C_6H_5C_3H_3$P_1 and $C_6H_5C_3H_3$A, and the C_7H_7+C_2H_2 channel at high temperatures (>1400 K). Indenyl's subsequent interactions with methyl, propargyl and vinylacetylene lead to the production of naphthalene, acenaphthylene and fluorene, respectively. Naphthyl radicals further participate in the formation of other bigger PAHs including 1-methyl naphthalene and 1-ethynyl naphthalene. Benzyl self-recombination and anthracene isomerization were analyzed to be the greatest contributors to phenanthrene formation. A small amount of phenanthrene is produced through $C_6H_5C_2H$+C_6H_5 and C_9H_7+C_5H_5 reaction channels. Finally, the findings will help researchers better understand how PAHs form during the combustion of surrogate fuels.

Acknowledgements

This project has received funding from the European Research Council (ERC) under the European Union's Horizon 2020 research and innovation programme (grant agreement n° 756785).

Disclosure statement

No potential conflict of interest was reported by the authors.

Funding

The work was supported by the H2020 European Research Council [grant agreement n° 756785].

References

Appleby, W. G., W. H. Avery, and W. K. Meerbott. 1947. Kinetics and mechanism of the thermal decomposition of n-heptane. *J. Am. Chem. Soc.* 69 (10):2279–85. doi:10.1021/ja01202a012.

Aribike, D., and A. Susu. 1988. Mechanistic modeling of the pyrolysis of n-heptane. *Thermochim Acta* 127:259–73. doi:10.1016/0040-6031(88)87502-6.

Aribike, D. S., and A. A. Susu. 1988. Kinetics and mechanism of the thermal cracking of n-heptane. *Thermochim Acta* 127:247–58. doi:10.1016/0040-6031(88)87501-4.

Bajus, M., V. Veselý, P. A. Leclercq, and J. A. Rijks. 1979. Steam cracking of hydrocarbons. 1. Pyrolysis of heptane. *Resour. Policy* 18 (1):30–37. doi:10.1021/i360069a007.

Chakraborty, J. P., and D. Kunzru. 2009. High pressure pyrolysis of n-heptane. *J Anal Appl Pyrolysis* 1 (86):44–52. doi:10.1016/j.jaap.2009.04.001.

Comandini, A., T. Malewicki, and K. Brezinsky. 2012. Online and offline experimental techniques for polycyclic aromatic hydrocarbons recovery and measurement. *Rev Sci Instrum* 83 (3):034101. doi:10.1063/1.3692748.

Curran, H. J., P. Gaffuri, W. J. Pitz, and C. K. Westbrook. 1998. A comprehensive modeling study of n-heptane oxidation. *Combust. Flame* 114 (1):149–77. doi:10.1016/S0010-2180(97)00282-4.

Davidson, D., M. Oehlschlaeger, and R. K. Hanson. 2007. Methyl concentration time-histories during iso-octane and n-heptane oxidation and pyrolysis. *Proc Combust Inst* 31:321–28. doi:10.1016/j.proci.2006.07.087.

Ferris, A. M., D. F. Davidson, and R. K. Hanson. 2018. A combined laser absorption and gas chromatography sampling diagnostic for speciation in a shock tube. *Combust. Flame* 195:40–49. doi:10.1016/j.combustflame.2018.04.032.

Garner, S., R. Sivaramakrishnan, and K. Brzezinski. 2009. The high-pressure pyrolysis of saturated and unsaturated C7 hydrocarbons. *Proc Combust Inst* 32:464–67. doi:10.1016/j.proci.2008.06.217.

Hamadi, A., L. Carneiro Piton, S. Abid, N. Chaumeix, and A. Comandini. 2022. Combined high-pressure experimental and kinetic modeling study of cyclopentene pyrolysis and its reactions with acetylene. In *Proc. Combust*, *Inst* doi:10.1016/j.proci.2022.07.023.

Hamadi, A., W. Sun, S. Abid, N. Chaumeix, and A. Comandini. 2022. An experimental and kinetic modeling study of benzene pyrolysis with C2–C3 unsaturated hydrocarbons. *Combust. Flame* 237:111858. doi:10.1016/j.combustflame.2021.111858.

Han, X., J. M. Mehta, and K. Brezinsky. 2019. Temperature approximations in chemical kinetics studies using single pulse shock tubes. *Combust. Flame* 209:1–12. doi:10.1016/j.combustflame.2019.07.022.

Held, T. J., A. J. Marchese, and F. L. Dryer. 1997. A semi-empirical reaction mechanism for n-heptane oxidation and pyrolysis. *Combust. Sci. Technol.* 123 (1–6):107–46. doi:10.1080/00102209708935624.

Hugoniot, P. H. 1887. Sur la Propagation du Mouvement dans les Corps et Spécialement dans les Gaz Parfaits (première partie) 57:3–97.

Hugoniot, P. H. 1889. Sur la Propagation du Mouvement dans les Corps et Spécialement dans les Gaz Parfaits (deuxième partie) 58:1–125.

Jin, H., L. Xing, J. Hao, J. Yang, Y. Zhang, C. Cao, Y. Pan, and A. Farooq. 2019. A chemical kinetic modeling study of indene pyrolysis. *Combust. Flame* 206:1–20. doi:10.1016/j.combustflame.2019.04.040.

Li, X., Z. Ma, E. Lv, Y. Dong, and X. Wang. 2021. Experimental and kinetic study of hydrocarbon fuel pyrolysis in a shock tube. *Fuel* 304:121521. doi:10.1016/j.fuel.2021.121521.

Manion, J. A., D. A. Sheen, and I. A. Awan. 2015. Evaluated kinetics of the reactions of H and CH3 with n-alkanes: Experiments with n-butane and a combustion model reaction network analysis. *J Phys Chem A* 119 (28):7637–58. doi:10.1021/acs.jpca.5b01004.

Mehta, J. M., W. Wang, and K. Brezinsky. 2022. Shock tube study of natural gas oxidation at propulsion relevant conditions. *Proc Combust Inst*. doi:10.1016/j.proci.2022.06.012.

Mertens, L. A., I. A. Awan, D. A. Sheen, and J. A. Manion. 2018. Evaluated site-specific rate constants for reaction of isobutane with H and CH3: Shock tube experiments combined with bayesian Model optimization. *J Phys Chem A* 122 (49):9518–41. doi:10.1021/acs.jpca.8b08781.

Miller, J. A., and S. J. Klippenstein. 2003. The recombination of propargyl radicals and other reactions on a C6H6 potential. *J Phys Chem A* 107 (39):7783–99. doi:10.1021/jp030375h.

Murata, M., and S. Saito. 1974. Prediction of initial product distribution from n-paraffin pyrolysis at higher temperatures by considering ethyl radical decomposition. *J. Chem. Eng. Jpn* 7 (5):389–91. doi:10.1252/jcej.7.389.

Murata, M., and S. Saito. 1975. A simulation model for high-conversion pyrolysis of normal paraffinic hydrocarbons. *J. Chem. Eng. Jpn* 8 (1):39–45. doi:10.1252/jcej.8.39.

Pant, K. K., and D. Kunzru. 1996. Pyrolysis of n-heptane: Kinetics and modeling. *J Anal Appl Pyrolysis* 36 (2):103–20. doi:10.1016/0165-2370(95)00925-6.

Pejpichestakul, W., E. Ranzi, M. Pelucchi, A. Frassoldati, A. Cuoci, A. Parente, and T. Faravelli. 2019. Examination of a soot model in premixed laminar flames at fuel-rich conditions. *Proc Combust Inst* 37 (1):1013–21. doi:10.1016/j.proci.2018.06.104.

Pilla, G., D. Davidson, and R. Hanson. 2011. Shock tube/laser absorption measurements of ethylene time-histories during ethylene and n-heptane pyrolysis. *Proc Combust Inst* 33:333–40. doi:10.1016/j.proci.2010.06.146.

Pyun, S., W. Ren, D. Davidson, and R. Hanson. 2013. Methane and ethylene time-history measurements in n-butane and n-heptane pyrolysis behind reflected shock waves. *Fuel* 108:557–64. doi:10.1016/j.fuel.2012.12.034.

Rankine, W. J. M. 1870. XV. On the thermodynamic theory of waves of finite longitudinal disturbance. *Philos. Trans. R. Soc. Lond* 160:277–88.

Shao, C., G. Kukkadapu, S. W. Wagnon, W. J. Pitz, and S. M. Sarathy. 2020. PAH formation from jet stirred reactor pyrolysis of gasoline surrogates. *Combust. Flame* 219:312–26. doi:10.1016/j.combustflame.2020.06.001.

Sun, W., A. Hamadi, S. Abid, N. Chaumeix, and A. Comandini. 2020. An experimental and kinetic modeling study of phenylacetylene decomposition and the reactions with acetylene/ethylene under shock tube pyrolysis conditions. *Combust. Flame* 220:257–71. doi:10.1016/j.combustflame.2020.06.044.

Sun, W., A. Hamadi, S. Abid, N. Chaumeix, and A. Comandini. 2021a. A comprehensive kinetic study on the speciation from propylene and propyne pyrolysis in a single-pulse shock tube. *Combust. Flame* 231:111485. doi:10.1016/j.combustflame.2021.111485.

Sun, W., A. Hamadi, S. Abid, N. Chaumeix, and A. Comandini. 2021b. Detailed experimental and kinetic modeling study of toluene/C2 pyrolysis in a single-pulse shock tube. *Combust. Flame* 226:129–42. doi:10.1016/j.combustflame.2020.11.044.

Sun, W., A. Hamadi, S. Abid, N. Chaumeix, and A. Comandini. 2021c. Probing PAH formation chemical kinetics from benzene and toluene pyrolysis in a single-pulse shock tube. *Proc Combust Inst* 38 (1):891–900. doi:10.1016/j.proci.2020.06.077.

Sun, W., A. Hamadi, S. Abid, N. Chaumeix, and A. Comandini. 2022. Influences of propylene/propyne addition on toluene pyrolysis in a single-pulse shock tube. *Combust* 236:111799. doi:10.1016/j.combustflame.2021.111799.

Sun, W., A. Hamadi, F. E. C. Ardila, S. Abid, N. Chaumeix, and A. Comandini. 2022. Insights into pyrolysis kinetics of xylene isomers behind reflected shock waves. *Combust. Flame* 244:112247. doi:10.1016/j.combustflame.2022.112247.

Tang, W., and K. Brezinsky. 2006. Chemical kinetic simulations behind reflected shock waves. *Int. J. Chem. Kinet.* 38 (2):75–97. doi:10.1002/kin.20134.

Wang, H., E. Dames, B. Sirjean, D. A. Sheen, R. Tango, A. Violi, J. Y. W. Lai, F. N. Egolfopoulos, D. F. Davidson, R. K. Hanson, et al. 2010. High-temperature chemical kinetic model of n-alkane (up to n-dodecane), cyclohexane, and methyl-, ethyl-, n-propyl and n-butyl-cyclohexane oxidation at high temperatures 2(2): 19. JetSurF version 2.0.

Wang, K., S. M. Villano, and A. M. Dean. 2015. Reactions of allylic radicals that impact molecular weight growth kinetics. *Phys. Chem. Chem. Phy* 17 (9):6255–73. doi:10.1039/C4CP05308G.

Yasunaga, K., S. Etoh, H. Yamada, H. Oshita, and Y. Hidaka. 2018. Modeling and experimental study on pyrolysis of isooctane and n-heptane behind reflected shock waves. *Chem. Lett.* 47 (6):747–50. doi:10.1246/cl.180154.

Yasunaga, K., H. Yamada, H. Oshita, K. Hattori, Y. Hidaka, and H. Curran. 2017. Pyrolysis of n-pentane, n-hexane and n-heptane in a single pulse shock tube. *Combust. Flame* 185:335–45. doi:10.1016/j.combustflame.2017.07.027.

Yuan, T., L. Zhang, Z. Zhou, M. Xie, L. Ye, and F. Qi. 2011. Pyrolysis of n-heptane: Experimental and theoretical study. *J.Phys. Chem. A* 115 (9):1593–601. doi:10.1021/jp109640z.

Zamostny, P., Z. Bělohlav, L. Starkbaumová, and J. Patera. 2010. Experimental study of hydrocarbon structure effects on the composition of its pyrolysis products. *J Anal Appl Pyrolysis* 87 (2):207–16. doi:10.1016/j.jaap.2009.12.006.

Zhang, K., C. Banyon, J. J. Bugler, H. Curran, A. Rodriguez, O. Herbinet, F. Battin Leclerc, C. B'chir, and A. Karl. 2016. An updated experimental and kinetic modeling study of n-heptane oxidation. *Combust. Flame* 172:116–35. doi:10.1016/j.combustflame.2016.06.028.